Bulletin of the Seismological Society of America, 91, 2, pp. 347–364, April 2001

Faster, Better: Shear-Wave Velocity to 100 Meters Depth from Refraction Microtremor Arrays

by John N. Louie

Abstract Current techniques of estimating shallow shear velocities for assessment of earthquake site response are too costly for use at most construction sites. They require large sources to be effective in noisy urban settings or specialized independent recorders laid out in an extensive array. This work shows that microtremor noise recordings made on 200-m-long lines of seismic refraction equipment can estimate shear velocity with 20% accuracy, often to 100-m depths. The combination of commonly available equipment, simple recording with no source, a wavefield transformation data processing technique, and an interactive Rayleigh-wave dispersion modeling tool exploits the most effective aspects of the microtremor, spectral analysis of surface wave (SASW) and multichannel analysis of surface wave (MASW) techniques. The slowness-frequency wavefield transformation is particularly effective in allowing accurate picking of Rayleigh-wave phase-velocity dispersion curves despite the presence of waves propagating across the linear array at high apparent velocities, higher-mode Rayleigh waves, body waves, air waves, and incoherent noise. Two locations illustrate the application of this technique in detail: coincident with a large accelerometer microtremor array in Reno, Nevada; and atop a borehole logged for shear velocity in Newhall, California. Refraction equipment could duplicate microtremor results above 3 Hz but could not estimate velocities deeper than 100 m. Refraction microtremor cannot duplicate the detail in the velocity profile yielded by a suspension logger but can match the average velocity of 10- to 20-m depth intervals and suggest structure below the 100-m logged depth of the hole. Eight additional examples from southern California and New Zealand demonstrate that the refraction microtremor technique quickly produces good results from a wide range of hard and soft sites.

Motivation

Comprehensive earthquake preparedness requires methods to rapidly assess the possibility of unusually strong shaking at a large number of sites. Estimating shallow shear-velocity structure can be an important component of site-response estimates of possible shaking (Borcherdt and Glassmoyer, 1992; Anderson *et al.,* 1996). The data and analysis presented in this article show how multichannel arrays of lightweight single 8-Hz vertical seismic refraction geophones can estimate surface-wave velocities to 100-m depths with very little field effort.

Such seismometers for refraction exploration weigh less than 1 kg each. Most universities and engineering consultants already possess seismic refraction systems that can digitally record between 12 and 48 geophones, or channels, simultaneously. This article shows how to easily deploy such commonplace equipment to record background noise, or microtremor, and how the data can yield surface-wave velocity dispersion measurements that constrain shallow shear-velocity structure. The success of these tests suggests that this technique will efficiently contribute to site-response assessments.

The refraction microtremor technique can only resolve velocity structure to depths of 100 m. Deeper constraints may require more conventional seismic survey methods and microtremor recordings by broader arrays of more sophisticated instruments (Horike, 1985). Satoh *et al.* (1997) made such analyses at the locations of unexpected damage from the 1994 Northridge earthquake. Liu *et al.* (2000) compared array results against deep borehole measurements at two California sites, finding that array aperture was the limiting factor in the depth resolution of surface-wave measurements.

A need for the rapid and inexpensive assessment of earthquake hazard at large numbers of sites has led to the development of several geophysical testing methods that do not require drilling. The well-known spectral analysis of surface waves (SASW) and microtremor array techniques both use surface-wave phase information to interpret shear-velocity or rigidity profiles. Other techniques that tried to

employ *P* waves or *S* body waves, for example, as presented in Williams *et al.* (1994), have not been as successful in matching ground-shaking or borehole data.

The SASW and MASW Techniques

Nazarian and Stokoe (1984) first described the SASW method to the earthquake engineering community. Sometimes referred to as CXW (Boore and Brown, 1998), SASW uses an active source of seismic energy, recorded repeatedly by a pair of 1-Hz seismometers at small (1 m) to large (500 m) distances (Nazarian and Desai, 1993). The seismometers are vertical particle-velocity sensors, so shear-velocity profiles are analyzed on the basis of Rayleigh-wave phase velocities interpreted from the recordings. The phase velocities are derived purely from a comparison of amplitude and differential phase spectra computed from each seismometer pair for each source activation, within a fast-Fourier-transform oscilloscope (Gucunski and Woods, 1991).

Since the original seismograms are not saved, and all interpretation is done in the frequency domain, the SASW method assumes that the most energetic arrivals recorded are Rayleigh waves. Where noise overwhelms the power of the artificial source, as is common in urban areas, or where body-wave phases are more energetic than the Rayleigh waves, SASW will not yield reliable results (Brown, 1998; Sutherland and Logan, 1998). The velocities of Rayleigh waves cannot be separated from those of other wave types in the frequency domain. Boore and Brown (1998) found that SASW models consistently underpredicted shallow velocities at the sites of six southern California borehole shear-velocity profiles, thus overpredicting ground motions by 10% to 50%.

The multichannel analysis of surface waves (MASW) technique (Park *et al.,* 1999) has been developed in response to the shortcomings of SASW in the presence of noise. The simultaneous recording of 12 or more receivers at short (1–2 m) to long (50–100 m) distances from an impulsive or vibratory source gives statistical redundancy to measurements of phase velocities. Multichannel data displays in a time-variable frequency format also allow identification and rejection of nonfundamental-mode Rayleigh waves and other coherent noise from the analysis.

Miller *et al.* (2000) were able to obtain excellent MASW results in the noisy environment of an operating oil refinery. Using both large and stacked small sources, they were able to acquire records dominated by fundamental-mode Rayleigh waves. They also attempted two-dimensional profiling for lateral anomalies in shear velocity by inverting many records along a profile. Such a profile represents much costly effort, similar to that needed for a high-resolution reflection survey, as a large source must be moved along and activated repeatedly at a large number of locations.

Simpler Acquisition and More Robust Analysis

The refraction microtremor method combines the urban utility and ease of microtremor array techniques with the operational simplicity of the SASW technique and the shallow accuracy of the MASW technique. By recording urban microtremor on a linear array of a large number of lightweight seismometers, the method achieves fast and easy field data collection without any need for the time-consuming heavy source required for SASW and MASW work. By retaining all the original seismograms and by applying a time-domain velocity analysis technique as is done in MASW, the analysis described in this article can separate Rayleigh waves from body waves, air waves, and other coherent noise. Transforming the time-domain velocity results into the frequency domain allows combination of many arrivals over a long time period and yields easy recognition of dispersive surface waves.

With sponsorship by the U.S. Geological Survey, the Southern California Earthquake Center, and the U.S. National Science Foundation; and through collaboration with colleagues from the Victoria University of Wellington, Shimizu Corporation, Kobe University, and the Disaster Prevention Research Institute of Kyoto University, this project carried out noise surveys at 10 locations in Nevada, southern California, and New Zealand. Three of these surveys were blind tests against other techniques. The Reno survey combined 1-km-wide arrays of 1-Hz sensors as used by Horike (1985) with 358-m linear arrays of 8-Hz and 4.5-Hz sensors at the northeast corner of the Reno/Tahoe International Airport. A 200-m linear noise and refraction array of 8-Hz sensors surveyed a ROSRINE borehole at the Newhall Fire Station in southern California. Also, linear analysis of existing 1-Hz array data compared favorably against SASW and seismic cone penetrometer profiles in the Parkway neighborhood of Wellington, New Zealand.

Method

The refraction microtremor technique is based on two fundamental ideas: (1) common seismic-refraction recording equipment, set out in a way almost identical to shallow *P*-wave refraction surveys, can effectively record surface waves at frequencies as low as 2 Hz; and (2) a simple, two-dimensional slowness-frequency (*p-f*) transform of a microtremor record can separate Rayleigh waves from other seismic arrivals and allow recognition of true phase velocity against apparent velocities.

Use of Seismic Refraction Recording Equipment

Two essential factors that allow exploration equipment to record surface-wave velocity dispersion, with a minimum of field effort, are (1) the use of a single geophone sensor at each channel, rather than a geophone group array, and (2) the use of a linear spread of 12 or more geophone sensor channels. Single geophones are the most commonly available type and are typically used for refraction rather than reflection surveying. The geophones with 8 Hz resonant frequency used at most of the ten sites tested here are on the

low end of the frequencies commonly found. They are not unusual among refraction equipment, however.

A geophone group array consists of several sensors wired together to sum electrically, producing a single recorder input channel. Petroleum-industry seismic-reflection surveys use geophone group arrays to cancel surface waves and other horizontally propagating energy and emphasize vertically propagating reflections. Because of the widespread use of group arrays, existing reflection records may not yield good results from these surface-wave analysis techniques. New data may have to be taken. If only geophone group array strings are available for new recording, they can be set in a cluster, or "potted," at one effective surface location. Alternatively, the strings might be stretched out perpendicularly to the trend of the refraction line, thus mitigating energy propagating across the line while enhancing the recording of waves traveling along the line.

A cluster test showed that common, compact seismic refraction sensors perform very well even if they are set as much as 20° off vertical. With no leveling needed, the setting of a 24-channel line of such geophones can take as little as one person-hour. Geophones are usually set below loose surface materials and buried under about 10 cm of tamped soil or set into the base of a slice cut into turf and pried open with a spade. It is easy to pound holes in asphalt pavement with a short length of 3/8-inch rebar to set the geophone spikes into, if unpaved areas are not available. These small holes are easily repaired with a quick-setting asphalt patching compound.

Another important component of this experimental setup was the use of a relatively long (8–20 m) interval between each geophone along the multichannel spread. The so-called takeout interval of the cables used for these tests is on the long side of those already in the market, but not unusual. The use of hundreds of meters of multichannel seismic recording cable can make deployment of this technique difficult in congested urban areas, where the cable would have to be protected at every vehicle crossing. An array of independent, stand-alone recorders is easier to deploy over a grid of streets. With careful examination of maps and some scouting, however, at least 200-m lengths of single blocks without cross streets can be found near almost any desired site.

The discussion here is restricted to recordings of single straight lines of geophones to evaluate the utility of the simplest deployment geometry. As a result, these analyses will contain energy at apparent phase velocities that are higher than the true phase velocities. The examples here demonstrate that the lower limit of the apparent phase velocities on these analyses can be recognized as the true phase velocity. With this ability, it is possible to record with a 200-m refraction cable at almost any site, even in very heavily urbanized areas.

Sensor Accuracy below Their Resonant Frequency. Many of the experiments reported here used a Bison Galileo-21 48-channel recorder and 8-Hz compact geophones. The Galileo-21 employs an instantaneous floating-point digitizer to 21-bit floating-point samples. Before digitization, the analog signals from the geophones pass through preamplifiers with configurable gain and filter settings. During tests of the system's response to low frequencies, using the 8-Hz geophones clustered together, setting the higher ranges of preamplifier gain yielded the most coherent recording of noise and microtremor frequencies below 5 Hz.

Table 1 gives representative correlation coefficients of combinations of preamp gain and frequency range for cluster noise records taken on the University of Nevada, Reno campus. The three columns of Table 1 list average correlation coefficients and their standard deviations between the 24 traces of cluster noise records after 0–5 Hz and 0–25 Hz low-pass filtering, and raw without filtering. These data show that all instrument preamp gain settings except zero can accurately record data above 5 Hz; including urban background noise and nearby sledgehammer impacts. Coherent microtremor at 4 Hz dominates the 0- to 5-Hz filtered noise records. A preamp gain of 40 or above will accurately record below 5 Hz, although raw or higher-frequency data will show digitizer clipping from nearby impacts.

A sledgehammer impact closer than 10 m from the geophone will cause physical clipping (pin the seismometer to the stops). No clipping was observed at lower gain for impacts more than 10 m from the cluster. The cluster records show poor but visible coherency below 5 Hz at 20 dB, suggesting that any data recorded with similar instruments might yield low-frequency velocities. Table 1 shows cross-correlation tests yielding correlation coefficients of 97.8 ± 2.0% among geophones in the cluster, at 0–5 Hz with a 60 dB gain. Background noise did not saturate digitally at such a gain, although hammer-blow recordings would.

Other recordings made under similar conditions with a Geometrics R24 seismograph yielding 24-bit integer samples and 12-Hz compact geophones (with the generous cooperation of J. Taber and T. Haver of the Victoria University of Wellington, New Zealand) did not need high preamplifier gain to record low-frequency microtremor accurately. These tests show that modern refraction geophone transducers, when properly coupled to the ground, can coherently record frequencies less than half their resonance frequency. Seismographs producing 12- and even 16-bit integer data, on the other hand, probably cannot record low-frequency microtremor without an analog high-cut filter.

The very great advantage of the refraction microtremor

Table 1
Low-Frequency Coherency Results from 8-Hz Geophones

Preamp Gain	0–5 Hz Filtered	0–25 Hz Filtered	Raw
20 dB	32.1 ± 10.2%	94.4 ± 1.6%	92.2 ± 1.6%
40 dB	92.9 ± 2.2%	96.4 ± 3.4%	96.3 ± 3.3%
60 dB	97.8 ± 2.0%	97.2 ± 2.4%	96.6 ± 2.4%

technique, from a seismic surveying point of view, is fourfold: it is very fast and inexpensive; it requires only standard refraction equipment already owned by most consultants and universities; it requires no triggered source of wave energy; and it will work best in a seismically noisy urban setting. Traffic and other vehicles, and possibly the wind responses of trees, buildings, and utility standards provide the surface waves this method analyzes.

Velocity Spectral (p-f) Analysis

The basis of the velocity spectral analysis is the p-τ transformation, or slantstack, described by Thorson and Claerbout (1985). This transformation takes a record section of multiple seismograms, with seismogram amplitudes relative to distance and time (x-t), and converts it to amplitudes relative to the ray parameter p (the inverse of apparent velocity) and an intercept time τ. It is familiar to array analysts as beam forming and has similar objectives to a two-dimensional Fourier-spectrum or f-k analysis as described by Horike (1985). Clayton and McMechan (1981) and Fuis *et al.* (1984) used the p-τ transformation as an initial step in P-wave refraction velocity analysis.

The p-τ transform is a simple line integral across a seismic record $A(x,t)$ in distance x and time t

$$A(p,\tau) = \int_x A(x, t = \tau + px)\, dx \tag{1}$$

where the slope of the line $p = dt/dx$ is the inverse of the apparent velocity V_a in the x direction. In practice, x is discretized into nx intervals at a finite spacing dx (here usually 8–20 m), so $x = jdx$ with an integer j. Likewise time is discretized with $t = idt$ (with dt usually 0.001–0.01 sec), giving a discrete form of the p-τ transform for negative and positive $p = p0 + ldp$ and $\tau = kdt$ called the slantstack:

$$A(p = p0 + ldp,\ \tau = kdt) = \sum_{j=0}^{nx-1} A(x = jdx,\ t = idt = \tau + px) \tag{2}$$

starting with a $p0 = -p_{\max}$. The parameter $p_{\max}$ defines the inverse of the minimum velocity that will be found, usually set at 200 m/sec but searched at 100 m/sec or less for particularly soft sites. The parameter np is effectively set to be 1 to 2 times nx. Here dp may range from 0.0001 to 0.0005 sec/m and is set to cover the interval from $-p_{\max}$ to $p_{\max}$ in $2np$ slowness steps. This will analyze energy propagating in both directions along the refraction receiver line. Amplitudes at times $t = \tau + px$ falling between sampled time points are estimated by linear interpolation.

The distances used in refraction microtremor analysis are simply distances of geophones from one end of the array. As described by Thorson and Claerbout (1985), the traces do not have to sample distance evenly, so the straight arrays analyzed here are for the convenience of field layout, not for the convenience of analysis. The intercept times after transformation are thus simply arrival times at one end of the array.

The p-τ transformed records contain, in the work here, 24 or 48 slowness traces, one or more per offset trace in the original x-t records. Each of these traces contains the linear sum across a record at all intercept times, at a single slowness or velocity value. The next step takes each p-τ trace in $A(p,\tau)$ (equation 2) and computes its complex Fourier transform $F_A(p,f)$ in the τ or intercept time direction:

$$F_A(p,f) = \int_\tau A(p,\tau) e^{-i2\pi f\tau}\, d\tau \tag{3}$$

for which the discrete Fourier transform with $f = mdf$ is

$$F_A(p, f = mdf) = \sum_{k=0}^{n-1} A(p, \tau = kdt) e^{-i2\pi mdfkdt} \tag{4}$$

although, in practice, the fast Fourier transform is mathematically equivalent but more efficient. Note that this is a one-dimensional transform that does not affect the slowness or p axis. Achieving good frequency resolution requires recording times longer than those typically used in seismic refraction work. For example, a time sampling dt of 0.001 sec requires a record length nt of at least 4000 samples, or 4 sec, for $df = 0.25$ Hz frequency resolution. In this work the refraction microtremor records range from 20 to 50 sec in length.

The power spectrum $S_A(p,f)$ is the magnitude squared of the complex Fourier transform:

$$S_A(p,f) = F_A^*(p,f)\, F_A(p,f) \tag{5}$$

where the * denotes the complex conjugate. This method sums together two p-τ transforms of a record, in both forward and reverse directions along the receiver line. To sum energy from the forward and reverse directions into one slowness axis that represents the absolute value of p, $|p|$, the slowness axis is folded and summed about $p = 0$ with

$$S_A(|p|,f) = [S_A(p,f)]_{p\geq 0} + [S_A(-p,f)]_{p<0} \tag{6}$$

This completes the transform of a record from distance-time (x-t) into p-frequency (p-f) space. The ray parameter p for these records is the horizontal component of slowness (inverse velocity) along the array. In analyzing more than one record from a refraction microtremor deployment, the individual records' p-f images $S_{A_n}(|p|, f)$ are added point-by-point into an image of summed power:

$$S_{\text{total}}(|p|,f) = \sum_n S_{A_n}(|p|,f) \tag{7}$$

So the slowness-frequency analysis has produced a record of the total spectral power in all records from a site, which

plots within slowness-frequency (*p-f*) axes. If one identifies trends within these axes where a coherent phase has significant power, then the slowness-frequency picks can be plotted on a typical period-velocity diagram for dispersion analysis.

The *p*-τ transform is linear and invertible and can in fact be completed equivalently in the spatial and temporal frequency domains (Thorson and Claerbout, 1985). The transform does act as a low-pass 1/*frequency* filter on the amplitudes in the data. However, this filtering does not distort or bias frequencies. The transform stacks along parallel lines to each intercept time, so there is no stretch or frequency distortion as there is for the normal-moveout or velocity stack along hyperbolae (Thorson and Claerbout, 1985). The transform does produce artifacts, however, smearing distance-limited or spatially aliased large amplitude waves over a large range of slownesses. This artifact does not prevent the identification of surface-wave dispersion, however.

McMechan and Yedlin (1981) developed the *p-f* technique and tested it against synthetic surface waves and reverberations seen on controlled-source multichannel seismic records. Park *et al.* (1998) applied the *p-f* technique to active-source MASW records. All phases in the record are present in the resulting (*p-f*) image that shows the power at each combination of phase slowness and frequency. Dispersive phases show the distinct curve of normal modes in low-velocity surface layers: sloping down from high phase velocities (low slowness) at low frequencies to lower phase velocities (high slowness) at higher frequencies. Miller *et al.* (2000) examine *p-f*-domain power spectra of MASW records along a profile to define lateral variations in dispersion curves and thus in shear velocities.

The distinctive slope of dispersive waves is a real advantage of the *p-f* analysis. Other arrivals that appear in microtremor records, such as body waves and air waves, cannot have such a slope. The *p-f* spectral power image will show where such waves have significant energy. Even if most of the energy in a seismic record is a phase other than Rayleigh waves, the *p-f* analysis will separate that energy in the slowness-frequency plot away from the dispersion curves this technique interprets. By recording many channels, retaining complete vertical seismograms, and employing the *p-f* transform, this method can successfully analyze Rayleigh dispersion where SASW techniques cannot.

Rayleigh Phase-Velocity Dispersion Picking

This analysis adds only a spectral power-ratio calculation to McMechan and Yedlin's (1981) technique, for spectral normalization of the noise records. The average power over all the slownesses may be orders of magnitude different from one frequency to another. This method takes the spectral ratio $R(|p|,f)$ of the power at each slowness-frequency combination against the average power across all slownesses at that frequency in individual *p-f* images $S_A(|p|,f)$, or in a summed image $S_{\text{total}}(|p|,f)$. Thus,

$$R(|p|,f) = S(|p|,f)np/[\sum_{l=0}^{np-1} S(|p| = ldp,f)] \quad (8)$$

with *np* being half of the original number of slowness steps 2*np*. In most cases the resulting spectral-ratio image shows maxima clearly aligned along a dispersion curve.

The ability to pick and interpret dispersion curves directly from the *p-f* images of spectral ratio parallels the coherence checks in the SASW technique (Nazarian and Stokoe, 1984) and the power criterion in the MASW technique (Park *et al.,* 1999). Picking phase velocities at the frequencies where a slope or a peak in spectral ratio occurs clearly locates the dispersion curve. Picks are not made at frequencies without a definite peak in spectral ratio, often below 4 Hz and above 14 Hz, where an identifiable dispersive surface wave does not appear. Often, the *p-f* image directly shows the average velocity to 30-m depth from the phase velocity of a strong peak ratio appearing at 4 Hz for soft sites or nearer to 8 Hz at harder sites.

Avoiding High Apparent Velocities. The use of linear geophone arrays in this technique means that an interpreter cannot just pick the phase velocity of the largest spectral ratio at each frequency as a dispersion curve, as MASW analyses effectively do. An interpreter must try to pick the lower edge of the lowest-velocity, but still reasonable, peak ratio. Since the arrays are linear and do not record an on-line triggered source, some noise energy will arrive obliquely and appear on the slowness-frequency images as peaks at apparent velocities V_a higher than the real in-line phase velocity *v*:

$$V_a = v/\cos(a) = 1/p \quad (9)$$

$$\text{or: } a = \cos^{-1}(vp) \quad (10)$$

with *a* being the propagation angle off the line direction.

The highly nonlinear relationship between *a* and *p* works in favor of interpreting accurate slowness (and velocity) from the appearance of wave energy in the $S(|p|, f)$ or $R(|p|, f)$ images. Energy within the images is arranged according to linear slowness *p*. Table 2 shows how energy arriving from different azimuthal angle *a* ranges will appear on a linear slowness *p* axis.

Each range of propagation angle *a* in the center column of Table 2 is the range within each of the four quadrants of the circle. Arrivals from azimuths a, $-a$, $180°-a$, and $180° + a$ will all be summed into the same $|p|$ trace of the $S(|p|,f)$ spectral-power image.

Assuming horizontally propagating energy arrives equally from all directions, Table 2 shows that 40.9% of the energy will be slantstacked into the *p* slowness traces that have 80–100% of the true slowness 1/*v*. In other words, 40.9% of the energy will appear at an apparent velocity $V_a = 1/p$ that is less than 1/0.80 = 125% of the true phase velocity. The rest of the energy is smeared thinly over the

Table 2
Angular Coverage of Slowness Intervals

Proportion of Inverse Velocity *vp*	Propagation Angle *a*	Coverage of 360° Energy
0–10%	90.0°–84.2°	6.3%
10–20%	84.2°–78.4°	6.4%
20–30%	78.4°–72.5°	6.6%
30–40%	72.5°–66.4°	6.8%
40–50%	66.4°–60.0°	7.1%
50–60%	60.0°–53.1°	7.6%
60–70%	53.1°–45.5°	8.4%
70–80%	45.5°–36.8°	9.7%
80–90%	36.8°–25.8°	12.2%
90–100%	25.8°–0°	28.7%
	Total:	100.0%

lower slowness ranges. Thus, at a particular frequency f within an $S(|p|,f)$ or $R(|p|,f)$ image, this technique tries to pick the phase velocity at the largest slowness $|p|$ (or smallest velocity) at which significant energy appears. Picking is done along a lowest-velocity envelope bounding the energy appearing in the $R(|p|,f)$ image.

It is possible to pick this lowest-velocity envelope in a way that puts confidence limits on the phase velocities, as well as on the inverted velocity profile. Making three picks at each frequency accomplishes this; first at a low phase velocity where the spectral ratio just begins to depart from the low ratios of incoherent noise; second at a best guess velocity where the ratio is rising steeply or has just leveled out; and third at a high velocity atop a spectral-ratio peak, which may be centered on an apparent velocity above the true phase velocity.

In crucial parts of the *p-f* images in the examples detailed subsequently, use of the discretized slowness values *dp* results in only 10% velocity change from one constant-slowness row to the next. So one row can include azimuths 30° away from the line direction (as at the bottom of Table 2), summing all energy arriving from nearly one-third of the full azimuthal circle. The remaining two-thirds is spread much more widely in slowness above the minimum-velocity envelope on the *p-f* image.

Picking a surface-wave dispersion curve along an envelope of the lowest phase velocities having high spectral ratio at each frequency has a further desirable effect. Since higher-mode Rayleigh waves have phase velocities above those of the fundamental mode, the refraction microtremor technique preferentially yields the fundamental-mode velocities. Higher modes may appear as separate dispersion trends on the *p-f* images, if they are nearly as energetic as the fundamental. Noticeable higher modes have appeared on the *p-f* analysis of an explosion refraction survey shot on a shallow, dipping pediment surface with a 2:1 velocity contrast (not shown).

Spatial aliasing will contribute to artifacts in the slowness-frequency spectral-ratio images. The artifacts slope on the *p-f* images in a direction opposite to normal-mode dispersion. The p-τ transform is done in the space and time domain, however, so even the aliased frequencies preserve some information. The seismic waves are not continuously harmonic but arrive in groups. Further, the refraction microtremor analysis has not just two seismograms, but 12 or more. So severe slowness wraparound does not occur until well above the spatial Nyquist frequency, about twice the Nyquist in most cases.

Shear-Velocity Modeling

The refraction microtremor method interactively forward-models the normal-mode dispersion data picked from the *p-f* images with a code adapted from Saito (1979, 1988) in 1992 by Yuehua Zeng. This code produces results identical to those of the forward-modeling codes used by Iwata *et al.* (1998) and by Xia *et al.* (1999) within their inversion procedure. The modeling iterates on phase velocity at each period (or frequency), reports when a solution has not been found within the iteration parameters, and can model velocity reversals with depth.

A graphical model-adjustment capability implemented around the modeling code allows rapid fitting of dispersion curves while adjusting the model with a computer mouse. This strategy results in quick testing of what model features are constrained by the dispersion-curve picks, and what depth-velocity trade-offs may exist. An interpreter can also interactively estimate the maximum depth of velocity constraint, and whether the data might rule out high-velocity transitions just below this depth. Because the refraction microtremor method does not rely on an inversion of dispersion picks for velocity structure, the forward-modeling part of the technique is the most dependent on the interpreter's skill and experience.

One way to lessen the modeling's dependence on the interpreter is to estimate the confidence limits of the velocity profile resulting from modeling by developing two models that fit the dispersion picks equally well. Shear-velocity profiles determined from dispersion picks are highly nonunique, and the interpreter should try to find at least two canonically different models giving the same dispersion curve. This approach is taken at the Reno site. However, defining canonical velocity profiles may be troublesome in engineering practice.

The interactive forward modeling of a dispersion curve by an experienced practitioner can yield more information about velocity constraints on a site than can an automated inversion procedure, such as that of Xia *et al.* (1999). The interactive modeling can avoid local minima in the objective error function that often result in false velocity inversions with depth, due to the equivalence problem that is inherent in the integrative nature of surface-wave velocities. Automatic inversions may be very effective in showing lateral variations along a profile, as in Miller *et al.* (2000), but often show oscillatory velocity anomalies that have artificially large magnitude.

In geophysical exploration work using other integrative fields such as gravity, magnetics, and resistivity, problems with automated inversions exaggerating anomalies have led to the widespread current practice of interactive forward modeling. Microtremor analysis done by Liu *et al.* (2000) completely avoids modeling of picked dispersions by simply comparing array dispersion data against dispersions forward modeled from borehole data. The interactive forward modeling of dispersion curves, though, is no slower than inversion procedures and allows the fitting of a simple model in less than a minute using popular computer platforms. The main difficulty with interactive modeling is to reduce the process of testing hypotheses and estimating confidence limits to a set of practical procedures that will not require extensive retraining by practitioners.

A simple method, more independent of the observer than developing a set of canonical models, is to fit models to the high- and low-velocity confidence limits of the dispersion picks. This procedure will produce extremal velocity profiles at the limits of the velocity range allowed by the dispersion data, a technique discussed for the Reno and Newhall examples below. With 95–99% of the minimum-velocity energy in the *p-f* images usually falling between the picked velocity extremes, there is similar confidence in the velocity ranges produced.

If higher-mode Rayleigh dispersion picks have been made, those can be modeled as well with the codes employed here. Another possible problem is the lack of information on *P*-wave velocities or densities in modeling Rayleigh dispersion curves. All of the modeling done for this article has assumed a Poisson ratio of 0.25, which is often far from the truth in shallow soils. Experimentation with the interactive modeling tool suggests that even huge changes in Poisson ratio or density will only change modeled shear velocities by less than 10% in the process of fitting Rayleigh-wave velocity spectra. Lay and Wallace (1995, p. 122) show that the Rayleigh phase velocity in a half space will change only from 89% to 95% of the shear velocity, as the Poisson ratio ranges from 0.1 to 0.4.

These factors suggest that Rayleigh dispersion curves are good indicators of shear-velocity structure and poor indicators of shallow *P*-velocity structure. A Jacobian analysis of Rayleigh dispersion inversion by Xia *et al.* (1999) supports this suggestion. Liu *et al.* (2000) also maintain that Rayleigh phase-velocity measurements can only constrain shear velocity. Since the refraction microtremor method uses essentially phase information from multichannel seismic recordings to estimate surface-wave phase velocities, determination of near-surface shear velocities is an attainable goal.

Results

Described here in detail are two tests of the refraction microtremor technique, done at locations where the most definitive corroborating data exist. The first test was against a more traditional accelerometer microtremor array (as in Horike, 1985; or Liu *et al.,* 2000) in Reno, Nevada. The second test was against the shear-velocity suspension log of a 100-m-deep borehole in Newhall, California. Described in less detail subsequently is the application of this technique at eight other locations in Wellington, New Zealand, and in southern California. This *p-f* analysis technique has also been applied extensively to explosion refraction records.

In all trials the method has produced reasonable shear-velocity results to 50–150 m depth, in good agreement with all available data. However, the two cases discussed first are those for which the best shear-velocity data from independent measurements were available. They were effectively blind prediction tests, as was the work of Liu *et al.* (2000), since the independent data were not examined before refraction microtremor results were developed. True blind prediction has not been attempted, however; it would require drilling and logging of a borehole only after refraction microtremor results had been published.

Tests Against a Microtremor Accelerometer Array in Reno, Nevada

On 22 July 1997 and 18 October 2000, University of Nevada, Reno, staff and students performed linear refraction array recording tests on the property of the Reno/Tahoe International Airport, at the southwest corner of Rock Blvd. and Mill Street in Reno, Nevada (Fig. 1). The site is next to the north end of the airport's main runways and about 1 km north of a site at which the UNR Seismological Lab made recordings of aftershocks of the 12 September 1994 Double Spring Flat event (Ni *et al.,* 1997). The site is bladed soil and gravel fill, covered by organic materials and silt deposited by a major Truckee River flood in January 1997. The site is about 300 m south of the river.

In the 1997 test two arrays of 24 8-Hz geophones spaced at 15.24 m were spread out in approximately W–E and N–S directions from the intersection. Each geophone was planted in a hole 10 cm deep, covered with soil, and tamped lightly. The several 48-sec noise records recorded by the Bison Galileo-21 had a 4 msec sampling interval and a 60 dB preamplifier gain. Fieldwork for that test required more than 8 person-hours because of the use of 48 channels over a 720 m total array length.

The 2000 test placed one N–S array of 15 RefTek RT-125 Texan recorders, with 24-bit fixed-point digitizers and 4.5-Hz geophones (Figure 1). The geophones were spaced at 20 m for an overall array length of 280 m. Geophone plants were similar, and five 50-sec noise records were taken. Fieldwork for that test required only 4 person-hours.

Wave Sources. One of the records triggered in 1997 was at the time of an approximately 3000 kg ripple-fired excavation blast 16 km to the south. Synchronizing watches over a cell phone link with an observer at the blast site provided timing to ± 2 seconds. The N–S channel 1–18 section of the

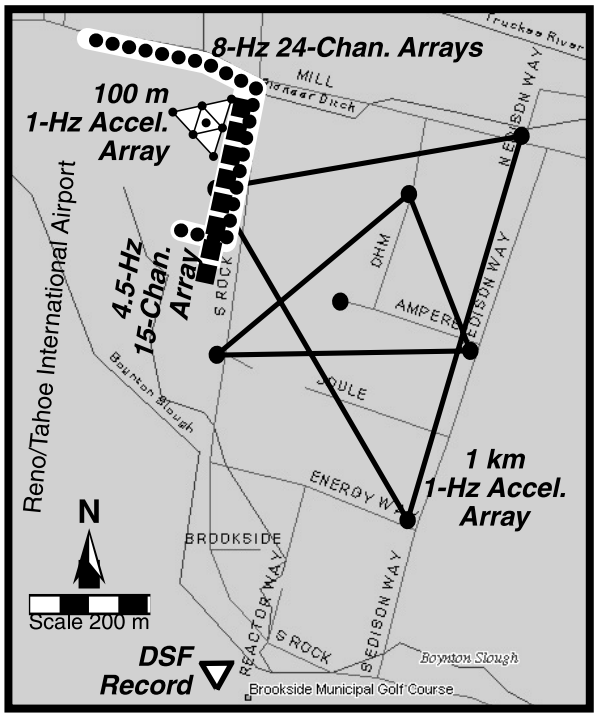

Figure 1. Map of microtremor experiment deployments near the Reno/Tahoe International Airport, western Nevada. The lines of 48 dots total show the 1997 placement of the 8-Hz single refraction geophones. Channels 1–18 extend south from the Rock and Mill intersection along Rock Blvd., with 19–24 turning west. Channels 25–48 extend west from the intersection along Mill St. The line of 15 rectangles shows the 2000 placement of the 4.5-Hz refraction geophones. The dots in triangular arrays show the locations of three-component accelerometers deployed by Iwata *et al.* (1998). The words labeling the airport are aligned with the location of the main runways in use during all the experiments. The major intersection between Rock Blvd. and Mill St., the nearby Truckee River, and the irrigation ditch flowing along the site also appear.

array (Fig. 1) pointed within 10° of the direction of the blast site. This record also used a high 60 dB preamplifier gain.

During both deployments, traffic was heavy through the adjacent major intersection and included all types of light and heavy vehicles. Vehicle speeds up to 20 m/sec can be identified on the records (not shown). In addition, the touchdown point of frequently landing Boeing 727 and 737 aircraft was only about 300–500 m distant. Some of the 1997 records were triggered to include aircraft landing and taking off (when the low-frequency jet rumble was loud). A 1.5-m-deep irrigation ditch was flowing vigorously at the site, less than 5 m from the 1997 W–E channels 25–36 (Fig. 1). A transcontinental freight rail line and Interstate Highway 80 are also $<$500 m north of the array.

Most of the energy in the 1997 microtremor records appears between 2 and 10 Hz, with the peak at 4.7 Hz. This result is surprising; considering the 8 Hz resonant frequency of the Mark Products geophones used, and the expected rapid decrease in their response at lower frequencies. It is consistent, however, with the low-frequency cluster test discussed previously, and it required the use of a high 60-dB preamplifier gain. The 2000 records using 4.5-Hz instruments recorded significant energy between 2.5 and 5.5 Hz, but most energy was between 8 and 20 Hz.

The 1997 deployment included sledgehammer refraction records taken from the intersection of the two 24-channel arrays. The high level of noise at this site together with the long spacing between geophones made the refraction times extremely difficult to pick. The only conclusion that can be made from them is that the average *P* velocity to 30-m depth is 890 $\pm$ 200 m/sec.

Analysis. Figure 2a shows results from the p-τ and Fourier transformation of five 48-sec noise records on the 1997 8-Hz refraction arrays, including the record from the 16-km-distant blast. Higher spectral ratios are darker in the images. Figure 2a also shows dispersion *p-f* picks and slowness errors. That case, as explained subsequently, used picks on the centers of spectral-ratio peaks. The errors represent the ranges of slowness within which the spectral-ratio peaks have a 95% chance of occurring. Each peak can be regarded as a Gaussian curve of relative power against frequency, so the error bars cover the range in which the spectral ratio is significantly elevated above the background. Note that the error bars must be at least two slowness rows in height on the *p-f* image, for a minimum slowness uncertainty of ± 0.213 sec/km. Since the vertical axis of the *p-f* plot is linear in slowness and nonlinear in velocity, the interpreted velocity error will be small for low-velocity picks and can be very large for high-velocity picks. The picks above 16 Hz have additional uncertainty.

Figure 2b shows the summed *p-f* power-ratio image from the five 4.5-Hz records taken in 2000. This image has less clear power-ratio peaking than the 8-Hz records image. It resembles more the concentration of power ratio along the lowest-velocity envelope with energy smeared along higher velocities as demonstrated in Table 2. Note that both the 8-Hz and 4.5-Hz *p-f* images (Figs. 2a, b) have a distinct peak at a high apparent velocity at 6 Hz, labeled V_a. At about 40% of maximum slowness, Table 2 suggests the source of that peak will be found at an angle a of 60° from the array trend. Iwata *et al.* (1998) saw energy arriving from the same azimuth and interpreted it as coming from the Interstate 80-US 395 freeway interchange 3 km from the site. As a result, Figure 2b is picked along a lowest-velocity envelope, with three picks at each frequency. As described previously, one is at the first rise of spectral ratio over the background at lower apparent velocities; the central pick is at the maximum slope in ratio versus slowness; and the third is atop a ratio peak. Clearly it was much more difficult to make picks below 3 Hz or above 15 Hz.

The normal-mode dispersion (down to the right in Fig.

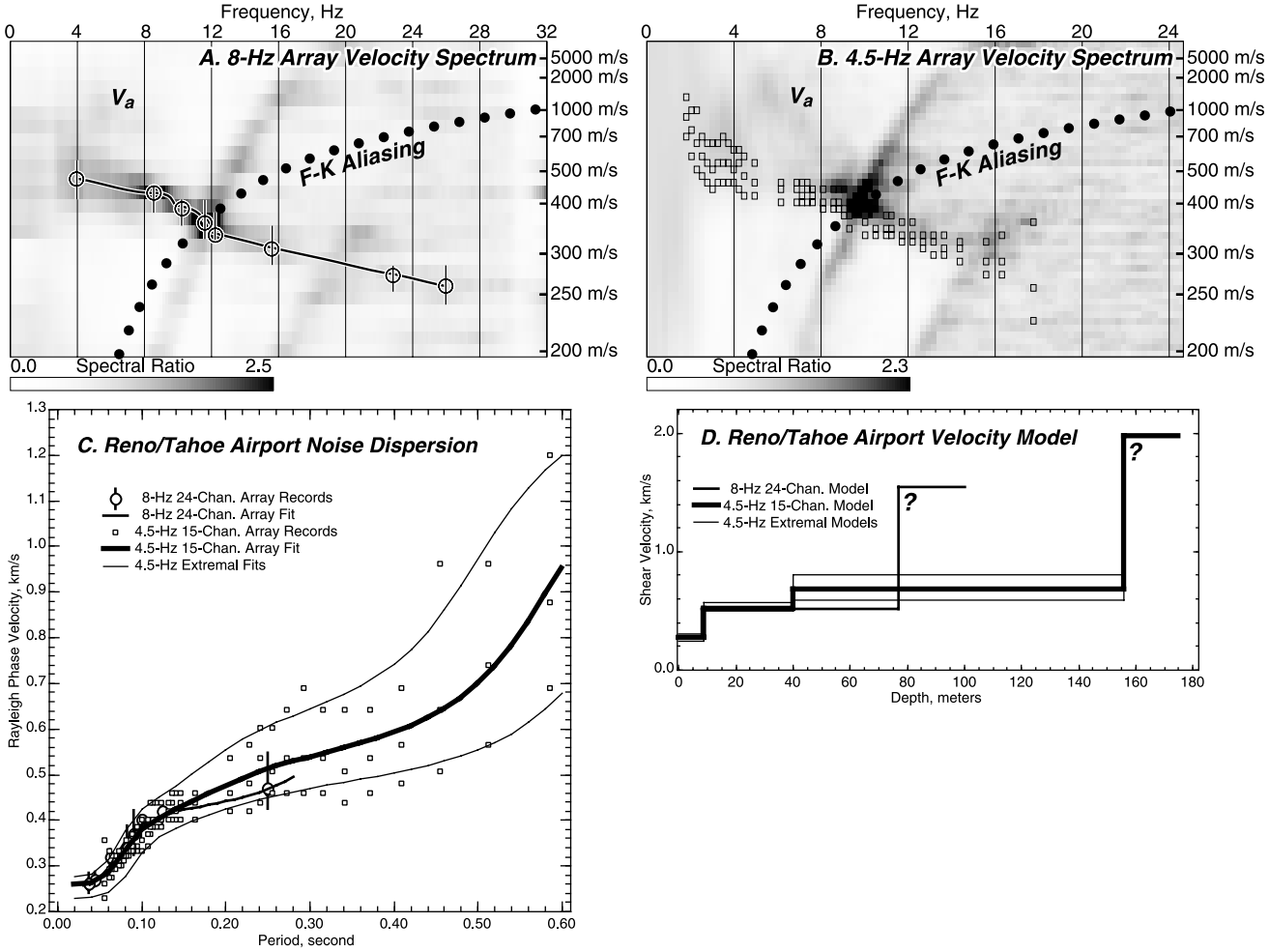

Figure 2. Analysis of shallow shear velocity near the Reno/Tahoe Airport, using recordings of microtremor noise on two arrays. The *p-f* images are linear from a slowness of zero (top edges) to 0.005 sec/m (200 m/sec minimum phase velocity, along the bottom edges). Higher spectral ratios are darker in the images. (a) Summed *p-f* transformation of five 48-sec 1997 records from the 8-Hz sensor arrays, with well-established *p-f* picks and errors (circles and bars). (b) Summed *p-f* transformation of five 50-sec 2000 records from the 4.5-Hz sensor array, with picks and extremal picks along the lowest-velocity envelope (small squares). *f-k* analyses would be spatially aliased below the dotted curves; but the *p*-τ transform can with care still yield useful phase velocities from this region. (e) Dispersion curves for all the picks, and matching fits. (d) Fit shallow shear-velocity models. The 8-Hz records picked to 4 Hz minimum frequency constrain velocities to 75-m depth. The 4.5-Hz records picked to 2 Hz constrain velocities to 150 m.

2a,b) is clear on both *p-f* images below the aliasing or Nyquist frequency (left of the heavy dots), where frequency-wavenumber (*f-k*) analysis such as Liu *et al.* (2000) would be spatially aliased. In the 1997 data from 8-Hz sensors (Fig. 2a) a spectral-ratio peak can be interpreted at frequencies as low as 3 Hz, but not below. In the 2000 data from 4.5-Hz sensors (Fig. 2b), both ratio peaks and the lowest-velocity envelope are clear down to 2.5 Hz, and the figure shows the less clear dispersion picks down to just below 2 Hz. The 4.5-Hz data allows picks to be made at each frequency column between 2 and 5.5 Hz, which much improves the low-frequency interpretation over that from the 8-Hz sensors.

Above the Nyquist frequencies, the picks also have larger slowness uncertainties. The trend of spectral-ratio peaks continues downward to the right, suggesting the typical surface-wave dispersion to lower velocities at higher frequencies. Spectral-ratio peaks trend up to 26 Hz in the analysis of 8-Hz data (Fig. 2a) and up to 16 Hz in the 4.5-Hz data (Fig. 2b). The *p-f* transform of the refraction microtremor technique never applies a Fourier transform to the spatial *x* axis. Thus, the images show that some information

can be recovered at high frequencies where *f-k* analyses would fail.

The strongest peaks of spectral ratio are at 12 Hz in Figure 2a and 10 Hz in Figure 2b. These peaks arise from waves that are spatially truncated by the edges of the arrays. The truncation leaves the smeared and frequency-shifted artifacts that arch up and to the right in both images, essentially artifacts of the p-τ transform (equations 1 and 2). Frequency wraparound smears the high-spectral ratio points in both plots subparallel to the dotted Nyquist curves. Clearly, however, these artifacts slope down to the left on the *p-f* plots and do not interfere with picking normal-mode dispersion trends.

In the areas of the *p-f* plots that would be aliased in an *f-k* analysis, the slantstack is still sensitive to the energy concentration of the group arrival across 12 or more traces in the record. This factor keeps the velocity range of the aliased, smeared peaks limited. The frequency wraparound and smearing show the frequency shift error of the peaks. These shifts do not extend beyond the limited shifts of the strong group arrival on Figure 2a at 12 Hz or on Figure 2b at 10 Hz. In this way, picks from the aliased areas of the velocity spectral plots could have 4–8 Hz of frequency error, up to 25%.

Examination of the 1997 raw blast record after 0–5 Hz low-pass filtering (not shown) identified surface wave arrivals with a 0.43 $\pm$ 0.03 km/sec group velocity and 0.86 to 1.3 km/sec phase velocity. These arrivals are not clearly separable in Figure 2a, although they contribute to a smear of moderately high spectral ratios at 6 Hz and below.

Apparent Phase Velocities. Figure 2a includes the spectral sum of four noise records and the 16-km distant blast record. The minimum apparent velocity, or true phase velocity, of the dispersed surface wave sums well. The sum included both the E–W and N–S parts of the arrays, showing the resulting coherence and preponderance of waves traveling near the true velocities. On both *p-f* images, V_a labels a significant spectral-ratio peak that does not contribute to the minimum-velocity interpretation. But the V_a peaks do not interfere with making the correct interpretation.

If one assumes an even distribution of energy arriving from all directions, over all these 48-sec records, then Table 2 makes clear the reason for the coherent summation at the true velocity. The nonlinearity of the cosine that divides the real velocity to produce the apparent velocity allows a third of the energy from many random directions to contribute to the observed peak, no more than 20% higher than the true velocity. The remaining two-thirds is spread much more widely in slowness and is visible in Figures 2a and b as a background of slightly higher spectral ratios, at velocities above the true dispersion curve. With the summing of spectra from records of two perpendicular linear arrays in Figure 2a, the nonlinear concentration of energy toward the true velocities on the *p-f* image is even more pronounced.

The superimposed line on Figure 2a traces the dispersion trend from 0.50 km/sec at 4 Hz down to 0.25 km/sec at 26 Hz. The slowness accuracy of this trend appears to be about the slowness sample interval of the p-τ transform (0.213 sec/km in that image). Thus, at the low-velocity end, the phase-velocity estimates should be accurate to within $\pm$0.015 km/sec. Frequency accuracy within this plot is not as good as the frequency sampling but can be $\pm$0.25 Hz or better, in picking spectral-ratio peaks outside the aliased area.

Velocity Modeling. Figure 2c graphs the picked dispersions, error bars, and extremal picks from both *p-f* images. It also shows the fits within the errors and extremes of synthetic dispersion curves from the models in Figure 2d. Extensive interactive testing with the forward-modeling application shows that picks constrain the 0–9 m depth shear velocity very well at 0.28 km/sec, the 9–40 m depth at 0.52 km/sec, as well as the 9 and 40 m depths of the velocity increases. The 0.68 km/sec velocity below 40 m can trade off against the depth and velocity of the deeper interface at 77–156 m (Fig. 2d). The aliasing and resulting frequency shifts of the picks above 12 Hz do not have a significant effect on the modeling.

The picks from the 8-Hz-sensor data, at 4-Hz minimum frequency, cannot constrain velocity below a 75-m depth. The interpreter, in the absence of other data, placed a 1.55 km/sec layer at 77-m depth. The picks from the 4.5-Hz-sensor data extend down to 2 Hz, allowing the interpreter to place a higher-velocity 1.98 km/sec interface deeper, at 156 m. Thus using lower-frequency sensors probably doubled the maximum depth of velocity constraint, to about 150 m (question marks on figure 2d). In both cases, the higher phase velocities picked at the lower frequencies demand a velocity increase at some depth below the depth of constraint. Being in essence depth-averaged velocities, the higher phase velocities constrain the ratio of the depth and velocity, but not either one individually.

In modeling the dispersion-curve picks of Figure 2c, the interpreter attempted to develop canonically different models that fit the data equally well. The differences in the two models presented in Figure 2d is in the number of shallow layers and in the depth and velocity of the deepest layer. The three-layer model presents an extreme hypothesis for the deepest layer, showing it at the minimum possible depth and minimum possible velocity. Both the test models, plus the models fitting the extremal picks, fit to nearly the same velocity at 9–77 m depths and also give a narrow velocity range for the shallowest 0- to 9-m layer. The three- and four-layer models have almost identical average velocities for the 0- to 30-m-depth range, of 456 and 448 m/sec, respectively.

Comparison with Accelerometer Results. In December 1997 colleagues from Shimizu Corp. and Kyoto and Kobe Universities tested at the Reno/Tahoe Airport site a nested-triangle array of seven 1-Hz, three-component accelerometers. This is the type of accelerometer array they have de-

ployed for microtremor noise recording in Japan and California (for example: Satoh *et al.,* 1997), and is almost identical to the techniques of Liu *et al.* (2000). They recorded both 100-m and 1-km-aperture arrays at the Reno/Tahoe Airport site (Fig. 1).

Each seismometer recorded independently, with timing provided by GPS clocks, so distributing the array over an area of several blocks was not difficult. Setting out each receiver, however, required a painstaking leveling process, as the 1-Hz accelerometers are far more sensitive to leveling errors than are the velocity sensors of the refraction equipment. The fieldwork for each array required more than 10 person-hours and used custom equipment costing more than $100,000.

Iwata *et al.* (1998) showed the results of their analysis for the airport site. They analyzed only vertical-component noise records. Total recorded time was about one hour; certain slices of their data several minutes long yielded good results in their moving-window *f-k* domain analysis (very much like the analysis presented by Liu *et al.* (2000). The frequency range of their phase velocity estimates (Fig. 3) overlaps that of the refraction experiments (from Fig. 2) between 2 and 7 Hz. At 3 Hz they determined a 0.475 ± 0.05 km/sec velocity, and at 7 Hz it was 0.45 ± 0.02 km/sec. From Figure 2a, the 8-Hz-sensor refraction microtremor pick at 4 Hz agrees with their results at 0.47 km/sec (Fig. 3). From Figure 2b, the 4.5-Hz-sensor refraction microtremor pick is higher at 0.51 km/sec, with extremes at 0.46 and 0.60 km/sec. At 8 Hz, the refraction microtremor picks are at 0.42 ± 0.02 km/sec. The lack of lower-frequency data prevents comparison against their results below 2 Hz. The data of interest for the prediction of shallow site amplification, from 4 Hz and up, are virtually identical.

Because of the close spacing and large number of channels allowed by the 8-Hz refraction equipment, it produces surface-wave dispersion most easily interpreted between about 7 and 16 Hz, as Figure 2a shows. The modeling in Figures 2c and 2d suggested that this range puts good constraints on shear velocities within 75 m of the surface. Dispersion is often interpretable in the *p-f* results at higher frequencies where an *f-k* analysis is impossible due to spatial aliasing. The refraction equipment could more accurately assess shear velocity at very shallow 1- to 10-m depths, while the 2D array of 1-Hz instruments was needed to estimate the velocity profile from 100-m to 1-km depths.

The amplification analysis of Ni *et al.* (1997), based on a nearby 30-m-deep acoustic log and weak-motion records, suggests similar shallow velocities, with modeled dispersion curves matching those of Iwata *et al.* (1998) above 3 Hz. Gravity work across the Reno basin by Abbott and Louie (2000a) shows a depth to andesite basement at the Reno Airport site of 400 m. Nearby water wells penetrating 200–300 m make it unlikely that the 77–156 m interface could be basement. It is more likely the base of Quaternary alluvium and the top of a Miocene-Pliocene diatomaceous sandstone that underlies the entire basin (Abbott and Louie, 2000a). Shallow models from noise recorded on refraction equipment could not derive basin sediment thickness here, although the lower-frequency accelerometer data of Iwata *et al.* (1998) could do so.

Test at the ROSRINE Borehole in Newhall, California

On 13 September 1996 the Resolution of Site Response Issues from the Northridge Earthquake (ROSRINE) project (*http://geoinfo.usc.edu/rosrine;* Nigbor *et al.,* 1997) collected an OYO suspension *P*- and *S*-wave velocity log at the Los Angeles County Fire Station in Newhall, California. In February 2000, with sponsorship from the Southern California Earthquake Center, and assistance from Los Angeles County Fire Dept. personnel and the County Flood Control District, University of Nevada, Reno staff located the site of the ROSRINE borehole and performed refraction and microtremor experiments.

The refraction microtremor experiment employed a 200-m-long array of 24 8-Hz refraction geophones along the asphalt-paved access road at the side of a 4-m-deep concrete-lined flood channel. The 200-m array was centered 4 m from the ROSRINE hole. Noise records 30 and 60 sec long and a reversed sledgehammer refraction profile were recorded. A 10-sec section of the first noise record taken appears in Fig-

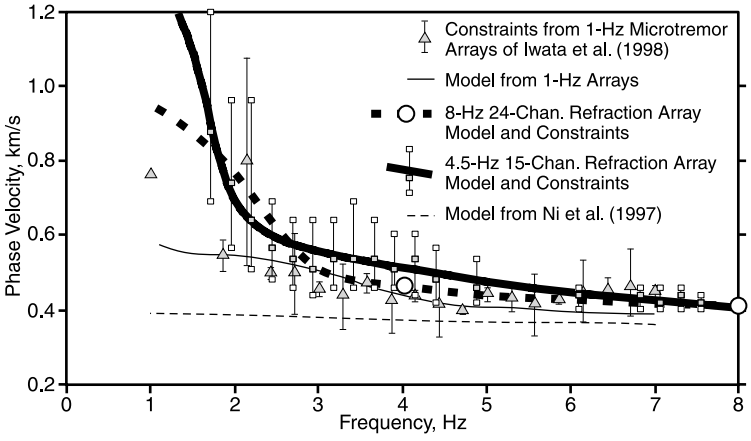

Figure 3. Comparison of phase-velocity spectra near the Reno/Tahoe Airport from three microtremor noise recording techniques. Triangles with error bars were picked from *f-k* analysis of broadband accelerometer array records by Iwata *et al.* (1998), yielding the model plotted with a thin solid line. Open circles and the thick dashed lines show the lower-frequency part of microtremor analysis using 8-Hz refraction equipment and the *p*-τ and Fourier transformation method, from Figure 2. Squares and a thick solid line show the results of the same analysis on the coincident array of 4.5-Hz refraction recorders. The thin dashed line is a model computed from a 30 m borehole log by Ni *et al.* (1997).

ure 4a. Using the same equipment as with the 8-Hz Reno/Tahoe Airport deployment, the microtremor fieldwork in Newhall required less than 6 person-hours, with a field crew of three. Time at the site was extended, however, by rain showers, recording of a large number of noise records, and by the hammer refraction recording.

Noise Sources. This part of Newhall is densely suburban, with heavily trafficked streets only 100–200 m apart, and fully built up. San Fernando Road, a six-lane artery, is only 75 m from the array. Frequent commuter trains were running 100 m away. The raw microtremor record in Figure 4a shows identifiable Rayleigh groups with 100–200 m/sec velocities, at a relatively high frequency of 18 Hz. The surface wave marked on Figure 4a, one example of the many present, probably originated close to the array. The lower-frequency microtremor is not easily seen in the figure, which includes frequencies up to 20 Hz.

Analysis. For the Newhall example, just the analysis of the first 30-sec noise record taken is shown here. If the refraction microtremor techniques can be sufficiently accurate on just one record, then prolonged field recording efforts are not needed. The *p-f* analysis of this 30-sec noise record is Figure 4b. From 3–12 Hz, the *p-f* image shows a clear energy cutoff at a minimum-velocity envelope. The energy of obliquely-propagating waves is broadly distributed across high apparent velocities above this envelope. Arrivals at many different apparent velocities form a broad ramp in spectral ratio, but the cutoff of high spectral-ratio values against the true phase-velocity envelope is clear from 3 to 12 Hz (as shown by Table 2). At frequencies below 3 Hz, and in the area of *f-k* aliasing, this envelope is not as clear. There are a few spectral-ratio peaks in these areas still aligned with the dispersion envelope.

The dispersion picks follow the lowest-velocity envelope at the base of the high spectral ratios in the image (Fig. 4b). The area of pick confidence is between the lowest velocity where spectral ratios rise above those of uncorrelated noise (white in Fig. 4b) and the higher velocity at the top of the ratio peak (black in Fig. 4b). The best pick was made within this range where the ratio slope is steepest, as for the Reno 4.5-Hz data in Figure 2b. The three phase-velocity values at one frequency constitute the dispersion pick (filled squares in Fig. 4c) and its uncertainty within extremal values (open squares in Fig. 4c). Dispersion picking is possible where an *F-K* analysis would spatially alias (right of the thick dashed line in Fig. 4b), although the *p-f* artifacts produce larger *p* uncertainties there.

Velocity Modeling. Figure 4c shows just the dispersion curve with increasing velocity uncertainty at larger periods, interactively modeled with the velocity profile of Figure 4d (bold line). The modeled profile is an excellent match to the ROSRINE logged shear velocity (thick gray line). The 8-m-thick shallowest layer with 210 m/sec shear velocity compares well with the log, which starts at a 2-m depth and varies from 178–238 m/sec to 8-m depth. The 370 m/sec modeled layer from 8 to 34-m depth averages across a strong gradient in the log from 219 to 685 m/sec over the same depth range. Below 34 m, the shear-velocity log has about 10% variability with a standard deviation of 77 m/sec but maintains the 105.2-m maximum logged depth, a 741 m/sec average. The 34 to 125-m-depth model layer has a velocity of 620 m/sec, which is just 16% low.

The bias of the interactive modeling process toward fewer layers, 7- to 100-m thick, is clear in this comparison. Since the phase-velocity dispersion data effectively integrate velocities over substantial depth ranges, modeling results could never match the detail of the shear-velocity log. In the log, velocities can change by 30% over a few meters. This lack of detail in the modeled velocity profile is no impediment to site-response evaluation, however. The amplification of earthquake waves by site conditions is also an integrative process. As long as the velocity results are accurate in terms of averages over 5 to 100-m depth ranges, accurate prediction of linear site amplification effects is assured (Borcherdt and Glassmoyer, 1992; Boore and Brown, 1998; Brown, 1998).

The uncertain longest-period picks of the dispersion curve (Fig. 4c) suggest a velocity increase at an interface below the 100-m maximum logged depth (question mark in Fig. 4d). However, the low-frequency dispersion picks cannot control the trade-off between the depth and velocity of this interface. Experimentation shows that many models could match the dispersions in Figure 4c. Both the depth and the velocity of the deepest layer are highly nonunique and very poorly determined at this site by the dispersions down only to 2 Hz. In this case, at least the ROSRINE log shows that the interface is deeper than 100 m. This fact suggests the refraction microtremor method could estimate velocity accurately to 100 m at this site.

The Newhall example demonstrates a simpler method of finding velocity constraints than that used for the Reno site. Developing a set of canonical models, essentially independent geological hypotheses, is too time-consuming for practical use. Modeling a single dispersion curve with the interactive tool is still a task that relies on some training, and tutorial exercises have been written to teach undergraduates how to perform the modeling effectively.

A top-down approach is most effective, matching phase velocities with layer velocity adjustments, starting at the surface layer (e.g., fitting the picks on Fig. 4c below 0.1-sec period first). Cusps and increases in slope of the dispersion curve (as at 0.12 sec, 0.25 sec, and 0.45 sec in Fig. 4c) are matched by adjusting layer thicknesses. Following such a procedure, it is possible to model velocities in about one minute, since only a small number of layers is used.

Here the extremal velocity limits are found by fitting not only the best picks (filled boxes on Fig. 4c) but also, separately, the highest-velocity picks, and the lowest-velocity picks of the confidence limits (open squares on Fig. 4c). This procedure results in three models, one central and two

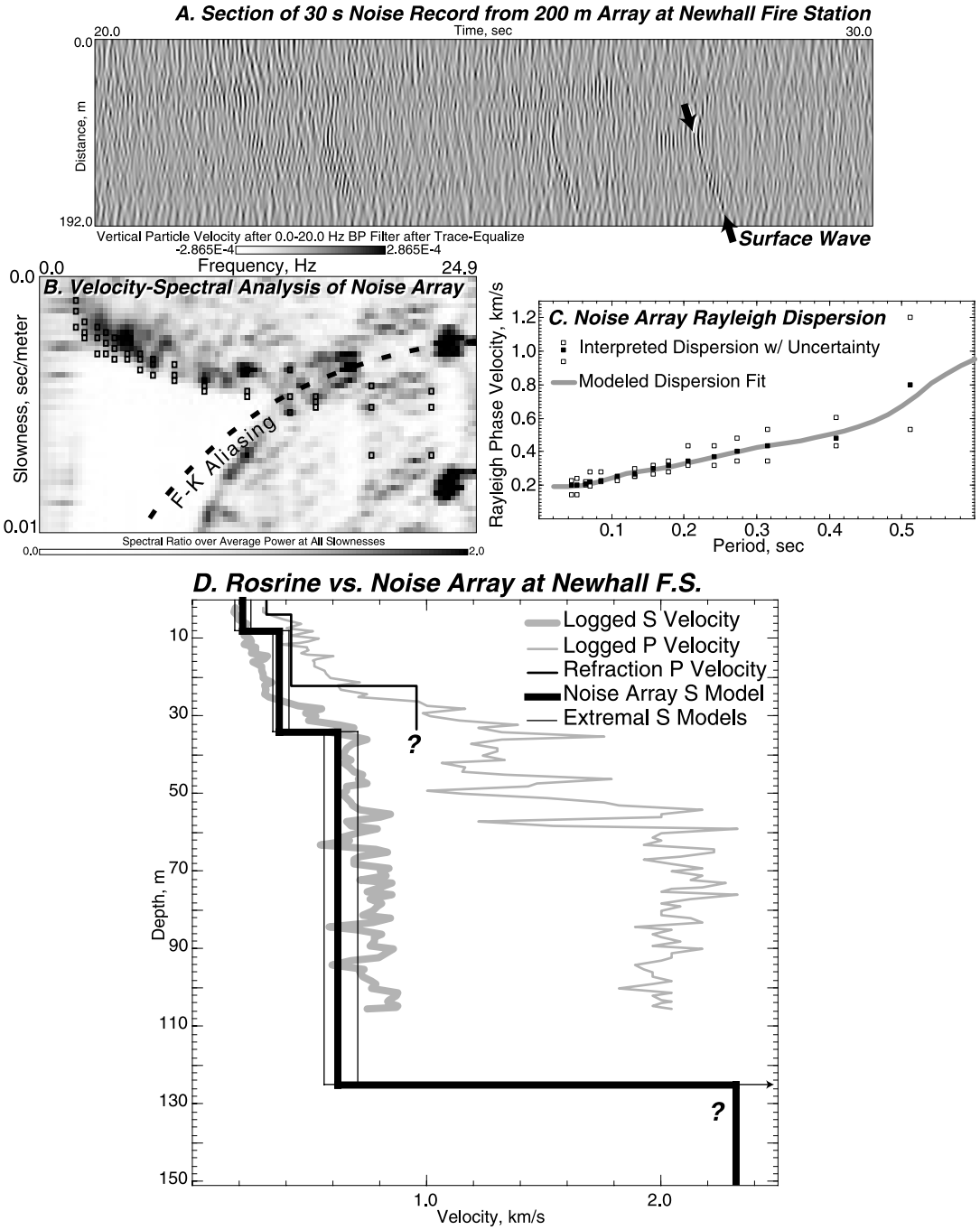

Figure 4. Demonstration of a 200-m linear array of 8-Hz seismic-refraction geophones, recording microtremor noise (a) at the Newhall Fire Station, southern California, and analyzed with the slowness-frequency (*p-f*) technique (b). The arrows on (a) point to one example of the many surface waves that can be seen in the record. Rayleigh-wave phase-velocity dispersions (c) lead to a model velocity profile (d) that can match suspension-logger shear-velocity results from the ROSRINE borehole there. Refraction *P* velocity below 30 m and microtremor shear velocity below 110 m are very poorly constrained (question marks).

that represent the upper and lower-velocity extremes of confidence in the pick of the central model. The thin lines on Figure 4d show the velocity profiles that result from this procedure. For the poorly constrained deepest layer (question mark in Fig. 4d), the minimum extremal model had the same velocity as the central model, while the maximum extremal model had a velocity of 3.5 km/sec, off the plot. For these data adjustment of layer thicknesses was not necessary in the process of creating the extremal models.

P-*Wave Refraction Results.* The refraction experiments conducted at Newhall show a shallow *P*-wave velocity of 328–408 m/sec. At 23-m depth, the *P*-wave velocity increases to 970 m/sec (thin black line in Fig. 4d). These values also agree well with the OYO suspension *P*-velocity log (thin gray line in Fig. 4d). Naturally a simple refraction interpretation cannot yield the detail of the suspension log. But the velocities and refractor depth agree well with the steep velocity gradient in the log from 26- to 34-m depth.

Both the 23-m deep *P*-wave refractor and the 34-m deep increase in shear velocity may represent the same interface, possibly a transition to more consolidated or clay-rich Quaternary alluvium. The interface is seen as both *P*- and *S*-wave velocity gradients over the 23- to 34-m depth range in the logs. The 11-m mismatch in depth between the refraction and shear-velocity modeling could be eliminated by biasing the refraction interpretation within its confidence limits or by inserting another layer into the shear-velocity model. First arrivals from 50 stacked hammer blows could only be seen to 130-m distances in this noisy area. As a result, the refraction data were not sensitive to either the logged *P*-velocity increase at 60-m depth or the bottom of Quaternary sediments at 125 m (or deeper) interpreted from the Rayleigh dispersion.

Stability of Data and Analysis. The record analyzed in Figure 4 is only the first of 14 noise records taken at the Newhall site. The experiment recorded 10 records 30 sec long, 5 with 2-msec sampling and 5 with 1-msec sampling. Four additional records were 60 sec long, with 1-msec time sampling. Summed *p-f* images were computed of the five 2-msec-sampled 30-sec records, of the five 1-msec sampled 30-sec records, and of the four 60-sec records. The *p-f* images are very similar to the single-record image, except for the increased concentration of energy close to the true phase velocity as was seen in the Reno summed-record analysis.

Each summed *p-f* image was picked independently. The picks all agree well with the single-record picks of Figure 4c, with two exceptions. The summed-record picks show phase velocities 15% to 30% higher than the single-record picks between periods of 0.3 and 0.42 sec. This is the period range most sensitive to the velocity of the 34- to 125-m-deep layer, which was 16% slower in the single-record analysis than in the shear-velocity log. Modeling the picks from this summed-record *p-f* image gave the layer a 707 m/sec velocity, only 5% lower than the 741 m/sec average in the log.

The other exception arose in trying to alter how one of the summed-record *p-f* images was picked. The five 30-sec records with 1-msec sampling produced a *p-f* image that seemed more distinctly peaked along the true-velocity dispersion curve than the other images. Accordingly, it was picked not along the low-velocity envelope but atop the center of its spectral-ratio peaks (not shown). At periods between 0.22 and 0.38 sec, this procedure yielded phase velocities that were up to two times larger than the velocities picked from all other Newhall *p-f* images. Fitting the best picks at the ratio peaks yielded a velocity for the 34- to 125-m-deep layer of 993 m/sec, 34% higher than the 741 m/sec average of the shear-velocity log for that depth range. For a randomly oriented single, straight-line noise array, picking the lowest-velocity envelope appears to be the most accurate procedure.

Extremal models matching the dispersion-envelope pick confidence limits show high confidence that modeling has estimated velocities to 100-m depth with 15% accuracy at Newhall, comparable to the total variability of the logged shear velocity over 5-m depth ranges. Rayleigh phase-velocity dispersion modeling matches the logged shear velocity despite a significant increase in the Poisson's ratio at 50-m depth. With the match to logged velocities shown in Figure 4, the cheap and rapid linear-array microtremor technique promises almost the depth and velocity resolution of the SASW and MASW techniques, but at lower cost since no artificial energy source is needed.

Additional Tests

Wellington, New Zealand. Ground-shaking hazard assessments have been underway for some years in New Zealand's Wellington metropolitan area (e.g., Van Dissen *et al.,* 1992). Geotechnical surveys of shear-velocity profiles have only taken place in two suburbs underlain by particularly soft sediments, known as Parkway and Porirua. In the Parkway suburb, Duggan (1997) conducted gravity and triggered-source seismic-refraction and reflection surveys, but not noise recordings. These techniques revealed 75 m of low-velocity lacustrine sediments overlying Mesozoic greywacke basement. Yu and Taber (1998) recorded noise and local events on a temporary network of 24 1-Hz stations about 0.5 km across. Barker (1996) made seismic cone-penetrometer profiles at three sites in Parkway. Sutherland and Logan (1998) provide shear velocities to 20-m depth from SASW surveys at a site in Parkway.

Figure 5 compares a model developed from *p-f* analysis of noise records from Yu and Taber's (1998) 0.5 km array of 1-Hz stations against the geotechnical results. Arranging the 12 soft-site stations available from the array with *x* distances appropriate for detecting waves propagating to the north showed clear Rayleigh-wave dispersion between 1 and 5 Hz. The velocities fitting the dispersion give a 30-m average shear velocities of 305 m/sec, with a good match, at 90-m depth, to Duggan's (1997) 75-m basin depth from gravity and reflection.

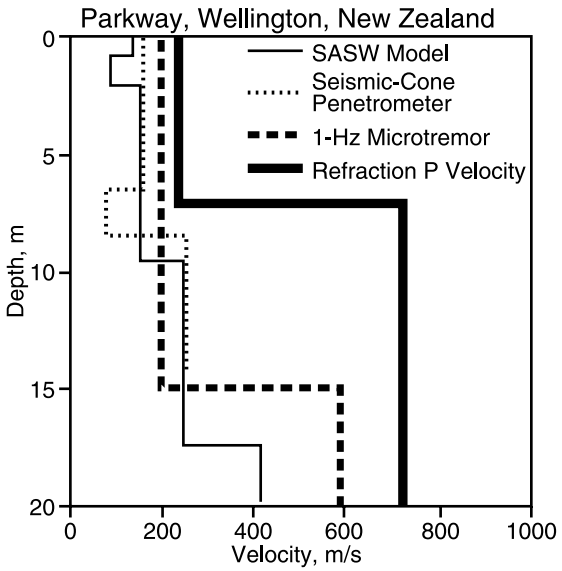

Figure 5. Comparison of velocity profiles estimated in the Parkway neighborhood of Wellington, New Zealand. SASW results from Sutherland and Logan (1998); seismic cone-penetrometer results from Barker (1996); and *P*-wave refraction velocities from Duggan (1997). The microtremor profile results from modeling of the *p-f* dispersion analysis (not shown) of records from a 1-Hz array deployed by Yu and Taber (1998). Dispersion analysis also finds the basin bottom at 75–90 m, beyond this plot to a maximum of 20 meters depth.

Figure 5 also shows the SASW and seismic cone-penetrometer results (from Sutherland and Logan, 1998). Given the large aperture of the 1-Hz array and the poor resolution of the refraction data, the microtremor result could not match the 17.5-m thickness of the low-velocity surface layer. But the microtremor surface-layer velocities just below 200 m/sec are a good match.

Taber and Richardson (1992) reported the highest strong-motion amplification measurement from Wellington in its Seatoun suburb. Although corroborating geotechnical measurements of velocity are not available from Seatoun, gravity measurements suggest a soft basin with 100-m maximum depth (McLoughlin, 1998). At Seatoun, a 24-channel array of 12-Hz geophones 200 m long was laid out along a beach in May 1999. Analysis of 16- and 32-sec noise records taken during the arrival of a southerly storm, with winds to 90 km/hr reported elsewhere in the city, yielded a clear dispersion curve from 22 to 10 Hz, with less clear but still interpretable dispersion from 10 Hz down to 4 Hz (not shown). Fitting the dispersion picks with two alternative velocity models found the end members of the range of models that will fit the data. Both end-member models agree with the prediction of 100-m basin depth by gravity (McLoughlin, 1998). The 30-m averaged shear velocities from the models range from 300 to 324 m/sec. Hammer refraction data taken before the arrival of the storm show a 30-m averaged *P* velocity of 1488 m/sec. Despite the low-rigidity condition of the Seatoun soils, the beach location guarantees their saturation with water. Thus, the *P* velocity could not be less than about 1500 m/sec.

Southern California. With sponsorship by the Southern California Earthquake Center, refraction microtremor measurements have been made at six additional sites in southern California. Most of these sites are on outcrops of hard rock hosting precariously balanced stones that have not been toppled by several of the most recent magnitude 8 earthquakes on the nearby San Andreas fault (Brune, 1999). The measurements were made to quantify the amount of deamplification that could be assigned to the higher velocities of precarious-rock sites. As a result, these measurements have tested the refraction microtremor technique across a very wide range of shallow velocity values. The linear-array noise recording technique, *p-f* analysis, and dispersion modeling techniques detailed previously all yielded well constrained results at all six additional sites. The conclusions of the earthquake-shaking study are presented elsewhere (Abbott and Louie, 2000b).

Being on hard rock, the additional six measurement sites are expected to be fast but have not been drilled. Although they cannot be compared with other shear-wave measurement techniques, as with Seatoun, a *P*-wave refraction result can be compared against the shear-wave modeling result. Sledgehammer refraction data were recorded at all the sites and analyzed for *P* velocity to 30-m depth using long-standing and simple techniques.

Figure 6 compares the *P*-wave refraction results against the shear-velocity models at all 10 sites discussed in this article. Figure 6 only compares 30-m-depth average velocities. For the graph, *P* velocities were divided by the square root of 3. Thus, if the Poisson ratio at a site is exactly 0.25, and the *P*-wave and shear-wave results agree perfectly, the site would plot on the 45° line angling up the middle of the graph.

In Figure 6 the hard-rock sites seem consistent with higher Poisson ratios, approaching 0.37. An alternative explanation would be that the linear-array microtremor analysis is underestimating the higher shear velocities by up to 20%. The soft-rock and soil sites, including those in Nevada, southern California, and New Zealand, all plot at a Poisson ratio indistinguishable from 0.25 (or with less than 10% shear-velocity error), except for Seatoun. That entirely water-saturated site cannot have a *P*-velocity much below 1500 m/sec, and so plots at a high, nearly fluid Poisson ratio. All the other sites are either in semi-arid regions or have been drained to some degree by water wells, and are not entirely saturated.

One way to interpret Figure 6 is that it shows that the refraction microtremor method will produce shear velocities accurate to 20% across an enormous range of velocity and Poisson's ratio. The technique is most accurate within 30 m of the surface, where most of the engineering interest in site

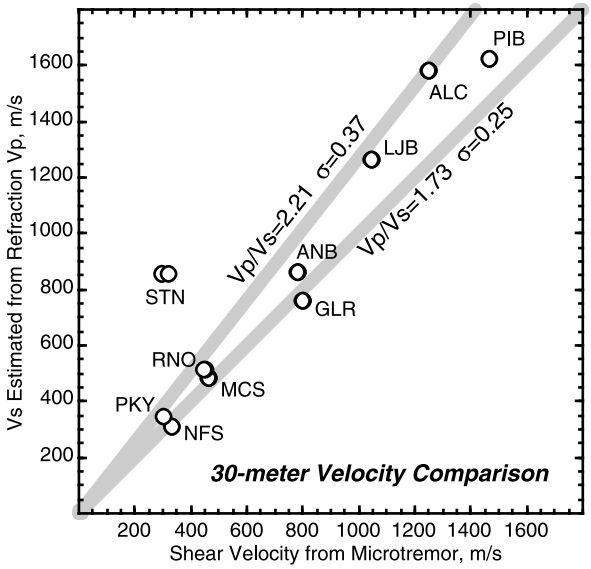

Figure 6. Comparison of 30-m averaged velocity estimates at ten sites. Shear velocities derived from microtremor modeling are plotted on the horizontal axis. Shear velocities estimated from coincident P-wave refraction results are plotted on the vertical, after assuming a Poisson ratio of 0.25 in converting to a shear velocity. In the Santa Clarita Valley and western Mojave Desert of southern California: NFS, Newhall Fire Station (Fig. 4); MCS, Mill Creek Summit; GLR, Gleason Road 0.5 km from MCS; ANB Antelope Buttes; LJB, Lovejoy Buttes; ALC, Aliso Canyon; and PIB, Piute Butte. In Nevada; RNO, Reno/Tahoe Airport (Fig. 1 and 2). In Wellington, New Zealand: PKY, Parkway (Fig. 5); STN, Seatoun.

conditions lies. Refraction microtremor will go beyond a 30-m depth, however, to produce useful constraints on shear velocity to a 100-m depth at most sites.

Conclusions

The 10 sites described in this article are all those tested with refraction microtremor to date, for which a corroborating velocity estimate is available from any other technique. Quiet rural sites (such as Piute Butte) do not yield refraction microtremor results as easily interpreted as results from noisy urban sites. Despite this variation in quality, every data set collected with this technique has yielded interpretable velocities. No site has been culled from the analysis here, and every data set collected has been analyzed.

The refraction microtremor method does not explicitly correct the apparent velocities of waves traveling obliquely to the array. Instead it relies on the stacking of waves traveling in all directions, the greater precision of the array for velocities along its length, and a procedure for picking the dispersion curve along a lowest-velocity envelope in the *p-f* images. This technique matched the shallower part of the results from microtremor recording in Reno of the type originated by Horike (1985) and yielded better shear-velocity estimates within 30 m of the surface. Comparison of these results against the shear-velocity log of the ROSRINE borehole at the Newhall County Fire Station proved the technique to be accurate, matching the log to within 15%. Eight additional tests in southern California and New Zealand show the refraction microtremor technique can quickly find the 30-m-average shear velocity to better than 20% accuracy.

These tests show that common seismic refraction equipment can yield accurate surface-wave dispersion information from microtremor noise. Configurations of 12 to 48 single vertical, 8–12 Hz exploration geophones can give surface-wave phase velocities at frequencies as low as 2 Hz and as high as 26 Hz. This range is appropriate for constraining shear velocity profiles from the surface to 100-m depths. The heavy triggered sources of seismic waves used by the SASW and MASW techniques to overcome noise are not needed, saving considerable survey effort. This microtremor technique may be most fruitful, in fact, where noise is most severe. Proof of this technique suggests that rapid and very inexpensive shear-velocity evaluations are now possible at the most heavily urbanized sites and at sites within busy transportation corridors.

In addition, limited resources for earthquake-hazard evaluation can now be stretched to measure at 3 to 10 times as many sites as was possible in the past. A possible application of this method would be to gather large numbers of 100-m shear-velocity profiles across mapped soil types used to predict regional shaking hazards (as by Borcherdt and Glassmoyer, 1992). Hazard classification schemes and hazard maps based on soil mapping could be verified against the velocity profiles. In addition, the multiple velocity measurements for each soil type would contribute a velocity variance to soil-type-based probabilistic seismic hazard mapping efforts.

Another application of this technique is that it is now possible to estimate shear velocities at one site for 10%–30% of the cost of SASW, MASW, borehole, or cone-penetrometer evaluations. In regions where the earthquake hazard or risk is not high enough to justify the cost of existing methods for site evaluation, this technique will allow a quick and affordable site study. The refraction microtremor technique requires as few as two person-hours, including all analysis, and equipment with a capital cost now as low as $10,000 (for a 12-channel refraction system). Even home builders might now be able to afford a shear-velocity evaluation at every home site. If engineers and builders find this technique useful, seismologists can look forward to an explosion in the number of available shallow site characterizations.

Acknowledgments

This research was supported in part by the U.S. Geological Survey National Earthquake Hazards Reduction Program under Contract Number N117292, with coinvestigators J. G. Anderson, F. Su, and Y. Zeng; as well

as by the Southern California Earthquake Center, with coinvestigators R. Anooshehpoor and J. Brune. SCEC is funded by NSF Cooperative Agreement EAR-8920B6 and USGS Cooperative Agreements 14-08-0001-A0899 and 1434-HQ-97AG01718. The SCEC contribution number for this article is 515. The W. M. Keck Foundation generously donated the seismic refraction equipment to the Mackay School of Mines, University of Nevada, Reno. Reftek 4.5-Hz Texan recorders and software were loaned by the IRIS/PASSCAL instrument center at New Mexico Tech, with training provided by S. Azevedo. T. Iwata, H. Kawase, T. Satoh, Y. Kakehi, and K. Irikura of the Disaster Prevention Research Institute, Kyoto University, Kobe University, and Shimizu Corporation graciously made the accelerometer deployments, performed data analyses, and also helped support the author's sabbatical research. Further crucial sabbatical assistance and collaboration were generously provided by E. Smith, M. Savage, J. Taber, T. Haver, M. Robertson, and R. Neal of the Victoria University of Wellington, New Zealand. Refraction instruments were deployed in Reno and southern California with valuable assistance from K. Smith, R. Anooshehpoor, R. E. Abbott, G. Ichinose, M. Herrick, M. Engle, A. Pancha, J. Skalbeck, and C. Mann. Caithness Power Corp. and Mike Tyler of Cal-Neva Drilling and Blasting kindly provided timing information on their 3000-kg construction blast. The Reno/Tahoe International Airport Authority generously provided access to the Reno site. The Los Angeles County Flood Control District and the Los Angeles County Fire Station in Newhall were very helpful in providing access to the ROSRINE site in Newhall, California.

References

Abbott, R. E., and J. N. Louie (2000a). Depth to bedrock using gravimetry in the Reno and Carson City, Nevada area basins, *Geophysics* **65,** 340–350.

Abbott, R. E., and J. N. Louie (2000b). High shear wave velocities under precarious rock sites might be enough to explain their existence near the San Andreas fault (abstract), *EOS Trans. AGU* **81,** no. 48, F821.

Anderson, J. G., Y. Lee, Y. Zeng, and S. Day (1996). Control of strong motion by the upper 30 meters, *Bull. Seism. Soc. Am.* **86,** 1749–1759.

Boore, D. M., and L. T. Brown (1998). Comparing shear-wave velocity profiles from inversion of surface-wave phase velocities with downhole measurements: systematic differences between the CXW method and downhole measurements at six USC strong-motion sites, *Seism. Res. Lett.* **69,** 222–229.

Borcherdt, R. D., and G. Glassmoyer (1992). On the characteristics of local geology and their influence on ground motions generated by the Loma Prieta earthquake in the San Francisco Bay region, California, *Bull. Seism. Soc. Am.* **82,** 603–641.

Brown, L. T. (1998). Comparison of Vs profiles from SASW and borehole measurements at strong motion sites in southern California, Master's Thesis, University of Texas, Austin, 349 pp.

Brune, J. N. (1999). Precariously balanced rocks along the Mojave section of the San Andreas fault, California: constraints on ground motion from great earthquakes, *Seism. Res. Lett.* **70,** 29–33.

Clayton, R. W., and G. A. McMechan (1981). Inversion of refraction data by wavefield continuation, *Geophysics* **46,** 860–868.

Duggan, E. B. (1997). Shallow seismic structure of Parkway basin, Wainuiomata, New Zealand, Bachelor's Thesis, School of Earth Sciences, Victoria University of Wellington, Wellington, New Zealand, 116 pp.

Fuis, G., W. Mooney, J. Healy, G. McMechan, and W. Lutter (1984). A seismic refraction survey of the Imperial Valley region, California, *J. Geophys. Res.* **89,** 1165–1190.

Gucunski, N., and R. D. Woods (1991). Instrumentation for SASW testing in *Recent Advances in Instrumentation, Data Acquisition, and Testing in Soil Dynamics,* Geotechnical Special Publ. No. 29: American Society of Civil Engineers, New York, p. 1–16.

Horike, M. (1985). Inversion of phase velocity of long-period microtremors to the S-wave-velocity structure down to the basement in urbanized areas, *J. Phys. Earth.* **33,** 59–96.

Iwata, T., H. Kawase, T. Satoh, Y. Kakehi, K. Irikura, J. N. Louie, R. E. Abbott, and J. G. Anderson (1998). Array microtremor measurements at Reno, Nevada, USA (abstract), *EOS Trans. AGU* **79,** no. 45, p. F578.

Lay, T., and T. C. Wallace (1995). *Modern Global Seismology,* Academic Press, San Diego, 521 pp.

Liu, H. P., D. M. Boore, W. B. Joyner, D. H. Oppenheimer, R. E. Warrick, W. Zhang, J. C. Hamilton, and L. T. Brown (2000). Comparison of phase velocities from array measurements of Rayleigh waves associated with microtremor and results calculated from borehole shear-wave velocity profiles, *Bull. Seism. Soc. Am.* **90,** 666–678.

McLoughlin, C. (1998). The Seatoun basin, Wellington, a geophysical investigation: evidence from gravity and electrical resistivity data, Bachelor's Thesis, School of Earth Sciences, Victoria University of Wellington, Wellington, New Zealand, 65 pp.

McMechan, G. A., and M. J. Yedlin (1981). Analysis of dispersive waves by wave field transformation, *Geophysics* **46,** 869–874.

Miller, R. D., C. B. Park, J. M. Ivanov, J. Xia, D. R. Laflen, and C. Gratton (2000). MASW to investigate anomalous near-surface materials at the Indian Refinery in Lawrenceville, Illinois, *Kansas Geol. Surv. Open-File Rept. 2000-4,* Lawrence, Kansas, 48 pp. (Electronic version at *http://www.kgs.ukans.edu/Geophysics/Reports2/Illinois.pdf*)

Nazarian, S., and M. R. Desai (1993). Automated surface wave method: field testing, *J. Geotech. Eng.* **119,** 1094–1111.

Nazarian, S., and K. H. Stokoe II (1984). In situ shear wave velocities from spectral analysis of surface waves in *Proceedings of the World Conference on Earthquake Engineering, Vol. 8,* San Francisco, 21–28 July.

Ni, S.-D., R. Siddharthan, and J. G. Anderson (1997). Characteristics of nonlinear response of deep saturated soil deposits, *Bull. Seism. Soc. Am.* **87,** 342–355.

Nigbor, R., C. Roblee, R. Pyke, J. Schneider, W. Silva, R. A. Steller, and M. Vucetic (1997). Resolution of site response issues from the Northridge earthquake (ROSRINE) (abstract), *Seism. Res. Lett.* **68,** p. 303.

Park, C. B., R. D. Miller, and J. Xia (1998). Imaging dispersion curves of surface waves on multichannel record in *68th Annual International Soc. Explor. Geophys.,* New Orleans, Sept. 13–18, *Expanded Abstracts,* p. 1377–1380.

Park, C. B., R. D. Miller, and J. Xia (1999). Multi-channel analysis of surface waves, *Geophysics* **64,** 800–808.

Saito, M. (1979). Computations of reflectivity and surface wave dispersion curves for layered media. I. Sound wave and SH wave, *Butsuri-Tanko* **32,** no. 5, 15–26.

Saito, M. (1988). Compound matrix method for the calculation of spheroidal oscillation of the Earth, *Seism. Res. Lett.* **59,** 29.

Satoh, T., H. Kawase, T. Iwata, and K. Irikura (1997). S-wave velocity structures in the damaged areas during the 1994 Northridge earthquake based on array measurements of microtremors (abstract), *EOS Trans. AGU* **78,** no. 46, 432.

Sutherland, A. J., and T. C. Logan (1998). SASW measurement for the calculation of site amplification, Earthquake Commission Research Project 97/276, Central Laboratories Report 98-522422, Lower Hutt, New Zealand, 22 pp.

Taber, J. J., and W. P. Richardson (1992). Frequency dependent amplification of weak ground motions in Wellington City and the Kapiti coast, Client report to Wellington Regional Council, New Zealand, 53 pp.

Thorson, J. R., and J. F. Claerbout (1985). Velocity-stack and slant-stack stochastic inversion, *Geophysics* **50,** 2727–2741.

Van Dissen, R. J., J. J. Taber, W. R. Stephenson, S. Sritharan, S. A. L. Read, G. H. McVerry, G. D. Dellow, and P. R. Barker (1992). Earthquake ground shaking hazard assessment for the Lower Hutt and Porirua areas, *Bull. New Zealand Natl. Soc. Earthquake Eng.* **25,** 286–302.

Williams, R. A., E. Cranswick, K. W. King, D. L. Carver, and D. M. Worley (1994). Site-response models from high-resolution seismic reflection and refraction data recorded in Santa Cruz, California, in *The Loma Prieta, California, Earthquake of October 17, 1989: Strong Ground*

Motion R. D. Borcherdt (Editor), *U.S. Geol. Surv. Prof. Pap. 1551-A,* A217–A242.

Xia, J., R. D. Miller, and C. B. Park (1999). Estimation of near-surface shear-wave velocity by inversion of Rayleigh wave, *Geophysics* **64,** 691–700.

Yu, J., and J. J. Taber (1998). Highly variable seismic amplification in Parkway, New Zealand (abstract), *EOS Trans. AGU* **79,** no. 4, F577–F578.

Seismological Laboratory and Dept. of Geological Sciences
Mackay School of Mines
The University of Nevada
Reno, NV 89557-0141
louie@seismo.unr.edu
http://www.seismo.unr.edu/us/refr.html

Manuscript received 23 June 2000.